RSC Advances

PAPER

View Article Online
View Journal | View Issue

Cite this: *RSC Adv.*, 2017, **7**, 24195

Zeolite cage-lock strategy for *in situ* synthesis of highly nitrogen-doped porous carbon for selective adsorption of carbon dioxide gas†

Chunfeng Xue,*[a] Hongye Zhu,[a] Tingting Xu,[a] Enyang Wang,[a] Bo Xiao,[b] Xuguang Liu,[a] Xiaogang Hao*[a] and Guoqing Guan[c]

Received 18th November 2016
Accepted 19th April 2017

DOI: 10.1039/c6ra26997d

rsc.li/rsc-advances

Nitrogen-doped porous carbon (NPC) was prepared by directly carbonizing zeolite ZSM-39 containing a structure-directing agent, tetramethylammonium chloride (TMACl), which also acted as a source of C and N for NPC. The cage-like pore of zeolite ZSM-39 acted as an ideal space for immobilizing the C and N species. The obtained NPCs have a high N content up to 18.14%. The quaternary N of template TMACl was transformed into pyridinic and pyrrolic/pyridonic N during the carbonization. NPCs were suitable for selective adsorption of CO_2 because of their unique ultra-micropores and abundant basic sites. The adsorption selectivity of CO_2 over N_2 was more than 12.1 (molar ratio). The CO_2 adsorption capacity of the unit surface area for a NPC-723 sample was calculated as 26.6 μmol m^{-2} at 0.93 bar and 273 K, which is one of the highest values among carbon adsorbents. Its excellent selectivity makes the NPC a good candidate for separating low concentrations of CO_2 in the purification of gas mixtures.

1. Introduction

The emission of greenhouse gases (carbon dioxide, methane, nitrous oxide, and ozone) causes problems with climate change and has become a widespread concern in recent years.[1] Carbon dioxide (CO_2) is one of the most persistent gases in anthropogenic gas emissions, which causes about 60% of global warming.[2] Moreover, it was applied as a resource in agricultural and food production and chemical industries and played a key role in sustainable economic development. Therefore, research on recycle and utilization of CO_2 has become crucial in solving problems with climate change, energy and environment issues.

Usually, the separation of CO_2 by an adsorption method is the fundamental step for its recyclable processing. Numerous porous materials such as zeolites,[3–5] metal oxides,[6,7] metal organic frameworks[8–10] and porous carbon have been used for this purpose. Among them, carbon-based materials have the advantages of a high specific surface area, pore volume, chemical inertness and easy regeneration. A few methods have been developed to obtain carbonaceous materials, such as an organic–organic co-assembly,[11] evaporation-induced self-assembly[12] and nanocasting hard template method.[13] Typically, the carbon source can be casted into mesostructured silica SBA-15 and carbonized at a certain temperature. This method has produced mesoporous N-free carbons with large pores, which are not very suitable for adsorbing CO_2. Alternatively, microporous N-free carbon with a high surface area was prepared by introducing and depositing a carbon precursor into zeolite Y at high temperatures.[14] To further enhance the adsorption capacity of CO_2, considerable efforts have also been made to introduce basic groups on the surface of carbons.[15] Nitrogen-doped porous carbons (NPCs) have been prepared *via* pyrolysis[16,17] or chemical vapor deposition[18,19] at 1023–1173 K, followed by impregnating/grafting organic amines or direct heat treatment of carbons with ammonia.[20,21] Porous doped carbons were synthesized by introducing a carbon source into the microporous template of zeolite 13X and Y, respectively.[22] For H_2O or H_2 adsorption, NPCs were prepared by depositing different carbon sources in zeolite Y, EMC-2, 13X, or β.[23,24] Moreover, additional C and N sources have to be provided for these deposition processes. In addition, the pore windows of zeolite templates mentioned above are too large to obtain the duplicated carbons with critical pores and show adsorption selectivity towards CO_2. In addition, the post-introduction technologies suffer from several drawbacks such as functional group losing, being time consuming and having a high cost.

Therefore, a well-chosen template is highly desirable for *in situ*, functionalized NPCs *via* an economic procedure without any casting or deposition process. Zeolite ZSM-39 belongs to the family of clathrasils, whose framework is built with packed eight ($5^{12}6^4$) and eight (5^{12}) cages.[25] Its unique cage-like, pore

[a]College of Chemistry and Chemical Engineering, Taiyuan University of Technology, Taiyuan 030024, Shanxi, China. E-mail: cfxue@fudan.edu.cn
[b]School of Chemistry and Chemical Engineering, Queen's University Belfast, Belfast, BT7-1NN, Northern Ireland, UK
[c]North Japan Research Institute for Sustainable Energy, Hirosaki University, Aomori, 030-0813, Japan

† Electronic supplementary information (ESI) available. See DOI: 10.1039/c6ra26997d

structure can deeply trap the used organic template, which cannot be completely removed by calcination.[26] Importantly, its pore window size is smaller than the dynamic diameter of N_2 (0.36–0.38 nm), thus promoting exclusive adsorption of CO_2 (0.33 nm). Therefore, ZSM-39 may be a good template candidate for immobilizing N-containing groups and preparing NPC with an ideal pore structure.

In this study, NPC materials were prepared with an *in situ*, carbonizing zeolite ZSM-39 containing a microstructure-directing agent, tetramethylammonium ions, followed by the removal of silica. Herein, the organic template was simultaneously used as a source of C and N for final NPC materials. The cages of zeolite ZSM-39 played an important role in immobilizing elemental N for the fabrication of desired NPCs. The obtained NPC showed a high N content up to 18.14%. The NPC-723 sample showed the highest CO_2 uptake of 1.93 mmol g^{-1} among the tested materials and good adsorption selectivity of 12.1 (molar ratio) for CO_2 over N_2.

2. Experiment

2.1 Chemicals

Colloidal silica (SiO_2, 6.05 mol L^{-1}) was purchased from Qingdao Chemical Factory. Tetramethylammonium chloride (TMACl, ≥ 99%), sodium hydroxide (NaOH, ≥ 96%), ammonium fluoride (NH_4F, ≥ 96%), and hydrofluoric acid (HF, 40% aq. solution) were purchased from China National Medicine Group Shanghai Corporation. All of the chemicals were used without further purification.

2.2 Synthesis of zeolite ZSM-39 template

Zeolite ZSM-39 was mainly prepared according to a reported method.[26] Simply, TMACl (12.86 g, 0.1162 mol) was used as a structure-directing agent and was first dissolved in 107 mL (5.9444 mol) of distilled water. Then, NH_4F (11.20 g, 0.2903 mol) was added with stirring at room temperature until a clear solution was formed. After that, SiO_2 (24 mL, 0.1452 mol) was added to the solution and further stirred for 1 h. Finally, the pH of the solution was adjusted to 10–11 using a 40% NaOH solution. The resultant mixture was stirred for another hour and then introduced into a Teflon-lined stainless steel autoclave. The sealed autoclave was heated at 473 K for 3 days. Subsequently, the solid sample was washed with distilled water and dried at 373 K overnight.

2.3 Preparation of NPC materials

Herein, NPC samples were fabricated by *in situ*, carbonizing the as-prepared zeolite ZSM-39. Briefly, zeolite ZSM-39 was directly carbonized under argon gas at a flow rate of 20 mL min^{-1} in a tube furnace at 723, 873 and 1173 K. The heating rate was 5 K min^{-1} and the dwelling time was 2 h at the designated temperature. The carbonized sample was immersed in a 20% HF solution with stirring for 12 h to remove the Si components. The black solid was washed at least 4 times with distilled water. Subsequently, the carbonaceous sample was dried at 393 K. The obtained samples were denoted as NPC-723, NPC-873, and NPC-1173, corresponding to their carbonization temperatures of 723, 873, and 1173 K, respectively.

2.4 Characterization

X-ray diffraction (XRD) patterns were collected using a D/Max-3B Rigaku X-ray diffractometer equipped with Cu-Kα radiation ($\lambda = 0.15406$ nm). The applied voltage and current were 30 kV and 40 mA, respectively. The samples were scanned from 5 to 45° at a scan rate of 8° min^{-1}. Textural properties were determined by N_2 sorption at 77 K using a volumetric technique on a JW-BK122W adsorption instrument. Before the measurements, all samples were degassed at 573 K in a vacuum for 12 h. The Brunauer–Emmett–Teller (BET) method was used to calculate the specific surface area. Pore volumes and pore size distributions were determined from the adsorption branches of isotherms using the Barrett–Joyner–Halenda (BJH) model. The Horvath–Kawazoe (HK) model was applied to evaluate the micropore volume and micropore size distribution. Fourier transform infrared (FT-IR) spectra of carbons were recorded on a Nicolet 6700 FT-IR spectrometer at room temperature in the range of 650–4000 cm^{-1} with potassium bromide as the window material. Morphologies of samples were obtained from a scanning electron microscope (SEM) HITACHI S-4800 instrument. Thermogravimetric (TG) curves were collected on a Netzsch STA 449 F5 TG/DTG instrument. About 6 mg of sample was placed onto an alumina crucible and heated at a ramp of 10 K min^{-1} from 30 to 950 °C in an airflow (100 mL min^{-1}) to analyze thermal stability. X-ray photoelectron spectra were collected on a Kratos Axis Ultra DLD spectrometer equipped with a monochromatic Al Kα X-ray source. The C, H, and N element content of NPCs were analyzed using a Vario EL III elemental analyzer. Raman spectroscopic data were recorded using a Renishaw in Via micro laser Raman spectrometer with Ar^+ laser (the wavelength is 514.5 nm) at an output power of 4 mW and scan range of 100–2000 cm^{-1} and a 10 s exposure.

2.5 Gas adsorption measurements

CO_2 uptake capacities of samples were evaluated on a JW-BK122W analyzer by collecting CO_2 isotherms from 0 to 0.93 bar at 253, 273 and 293 K. All the samples were first degassed at 573 K for 12 h. N_2 isotherms were also recorded in order to evaluate adsorption selectivity of NPC samples from 0 to 0.93 bar at 293 K.

3. Results and discussion

The XRD pattern of the as-prepared silica zeolite ZSM-39 exhibited typical peaks, indicating good crystallinity (Fig. 1a). The positions of the main diffraction peaks were identical with those of ZSM-39 clathrate compounds as previously reported,[26] indicating that a pure phase of zeolite ZSM-39 was prepared. The sample was directly carbonized in argon flow to convert the included organic template into a carbonaceous material. After the silica framework of carbonized ZSM-39 was etched by an HF solution, the black NPC samples were obtained. By changing the temperature from 723, 873, to 1173 K, samples NPC-723,

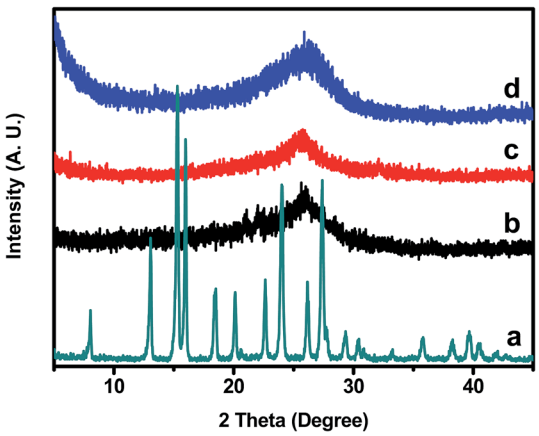

Fig. 1 XRD patterns of samples: (a) as-made ZSM-39, (b) NPC-723, (c) NPC-873, and (d) NPC-1173.

NPC-873, and NPC-1173 were respectively prepared. Their XRD patterns exhibited broad peaks at $2\theta = \sim 26^\circ$ indexed as the planes of turbostratic carbon[27] (Fig. 1b–d). The XRD patterns were different from those of a pristine ZSM-39 template, implying that NPC samples did not have the residuals of a zeolitic structure. Although most of TMACl template can undergo carbonization because of the spatial limitation imposed by the cage-like lock, the remaining species may not be enough to duplicate the desired zeolite structure during the carbonization. Carbonaceous species of an organic template could be immobilized under the assistance of zeolite ZSM-39 even at 1173 K. After a careful comparison, it was discovered that the intensity and sharpness of this peak became stronger at a higher temperature, implying a significant trend in the graphitization of NPCs.

Raman spectra of NPC-723, NPC-873 and NPC-1173 samples (Fig. 2) revealed a pair of broad bands at 1355 and 1590 cm^{-1}. Generally, the band at 1355 cm^{-1} is associated with the presence of disordered structure (D). Its intensity increased when the number of defects increased.[24] The graphitization (G) band at about 1590 cm^{-1} was closely related to the vibration in sp^2 bonded C atoms in a 2-dimensional hexagonal lattice.[24] For nanotube and pure graphitic carbon, the D band was absent, and only the G band appeared.[24] The intensity ratio of the D to G band (I_D/I_G) is generally used to illustrate the graphitization degree of a carbon material. Herein, the NPC-723 sample displayed the highest I_D/I_G ratio among the three samples (Fig. 2a), which was attributed to the low carbonization temperature. The I_D/I_G value of 0.95 for NPC-723 and a similar value of 0.94 for NPC-873 (Fig. 2b) implied a similar degree of graphitization. The lowest value of 0.88 was estimated for NPC-1173. Lower I_D/I_G values have been associated with higher degrees of graphitization.[28] Accordingly, the NPC-1173 sample exhibited the highest degree of graphitization among the three samples (Fig. 2c). The trend in the degree of graphitization agreed with those concluded from XRD patterns.

FT-IR spectra of all NPC materials were collected and summarized in Fig. 3. The broad bands at 3436 cm^{-1} were assigned to –OH group stretching vibrations and indicated the presence of structural water. The resolvable bands at 3220 and 3130 cm^{-1} for samples NPC-723 and NPC-873 can be assigned to N–H stretching vibrations (Fig. 3a and b).[29] However, they are difficult to identify for NPC-1173 after high temperature carbonization (Fig. 3c). Three weak bands around 2965, 2923, and 2860 cm^{-1} were assigned to the C–H stretching vibrations. The band at 1640 cm^{-1} was attributed to a C=N stretching vibration,[30] implying the possible N-heterocycle existing in the NPCs. The band around 1524 cm^{-1} was attributed to a bending vibration of N–H, and the band located at 790 cm^{-1} represented the out-of-plane N–H deformation vibration. In addition, the band around 1524 cm^{-1} for NPC-1173 was noticeably weaker than the other two samples (Fig. 3c). The bands at 1450 and 1500–1600 cm^{-1} were attributed to C=C stretching vibrations, implying the presence of aromatic rings related to the graphitization. The weak and broad band at 1263 cm^{-1} corresponded to the C–N stretching vibration. According to the observations above, the FT-IR spectra confirmed the co-existence of N–H, C=N and C–N species in the resultant NPC materials. Thus, it

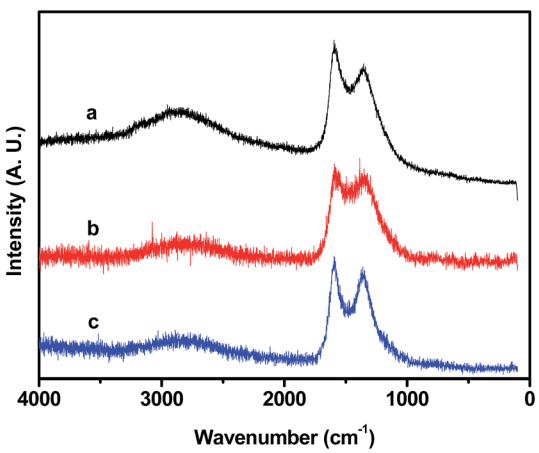

Fig. 2 Raman spectra of samples: (a) NPC-723, (b) NPC-873, and (c) NPC-1173.

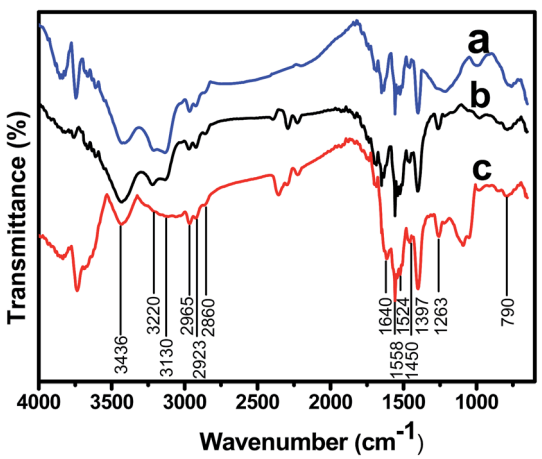

Fig. 3 FT-IR spectra of samples: (a) NPC-723, (b) NPC-873 and (c) NPC-1173.

Table 1 Elemental analysis results and textural properties of NPC samples[a]

Sample	C	N	H	S_{BET}, $m^2\ g^{-1}$	V_{Micro}, $cm^3\ g^{-1}$	V_T, $cm^3\ g^{-1}$
NPC-723	69.63%	18.14%	2.82%	53.3	0.019	0.168
NPC-873	76.68%	13.04%	1.55%	269.4	0.098	1.112
NPC-1173	95.37%	1.11%	1.01%	51.0	0.020	0.169

[a] Note: S_{BET}: specific surface area calculated according to BET method; V_{Micro}: pore volume derived from micropores; V_T: total pore volume.

was concluded that the *in situ*, zeolite cage-lock strategy could immobilize not only the inert C element but also the active N element for obtaining functionalized carbonaceous materials.

The presence of N, C, and H elements was further confirmed and quantified by elemental analysis. According to the analysis results, the N content of NPC-723 approached 18.14% and the C content was about 69.63% (Table 1). The N/C molar ratio of the NPC-723 sample was calculated as 1 : 4.48 and was very close to that (1 : 4) of the organic template TMACl. The results further demonstrated that the zeolite cage-lock strategy was successful in immobilizing most of the N elements from the template into final NPC samples. As the carbonization temperature increased, the C content of the NPC-1173 sample reached up to 95.37%, while the N content dropped to 1.11%. The further enhanced carbonization agrees well with the findings drawn from the XRD pattern and Raman spectra. However, the clear drop in N content made us aware that most of N species escaped from the cages of zeolite ZSM-39 at high temperatures.

The textural properties of NPCs were analyzed using N_2 adsorption at 77 K and are summarized in Table 1. NPC-723 sample mainly exhibited adsorption at low relative pressure $P/P_0 \leq 0.05$ due to the capillary filling of micropores (Fig. 4a). These results imply that a part of the micropores duplicated from the ZSM-39 template was accessible to N_2 molecules. Its BET surface area was calculated as only 53.3 $m^2\ g^{-1}$. The main reason for this low surface area was that the window sizes of some cage-like pores were too small to adsorb an N_2 molecule. To some extent, the small window size was critical and important for selectively adsorbing CO_2 from the mixture of N_2 and CO_2. The pore volume derived from the adsorption branch of isotherms was 0.168 $cm^3\ g^{-1}$ for NPC-723. According to the pore size distribution derived from the adsorption branches of isotherms using the BJH model, the pore diameter of NPC-723 was centered at about 3.0 nm (Fig. 5Aa). The HK method was used to calculate the micropore size distribution, and the pore diameter was centered at 1.0 nm (Fig. 5Ba inset).

After being carbonized at 873 K, the obtained NPC-873 material exhibited a type IV isotherm with significant adsorption in $P/P_0 \leq 0.05$ and a broad hysteresis loop above $P/P_0 = 0.45$ (Fig. 4b), implying a hierarchical structure composed of micro- and mesopores. The results indicated that the micropores

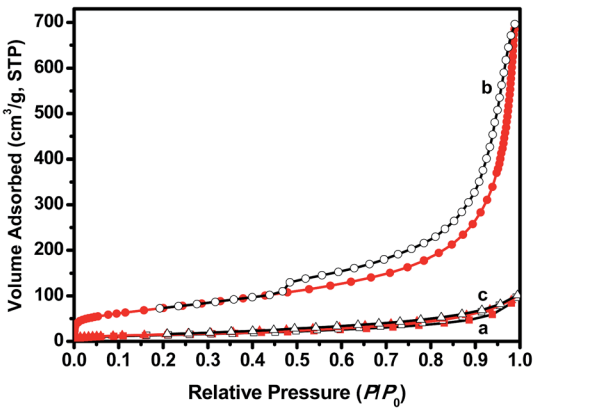

Fig. 4 N_2 sorption isotherms of samples: (a) NPC-723 (square), (b) NPC-873 (circle) and (c) NPC-1173 (triangle).

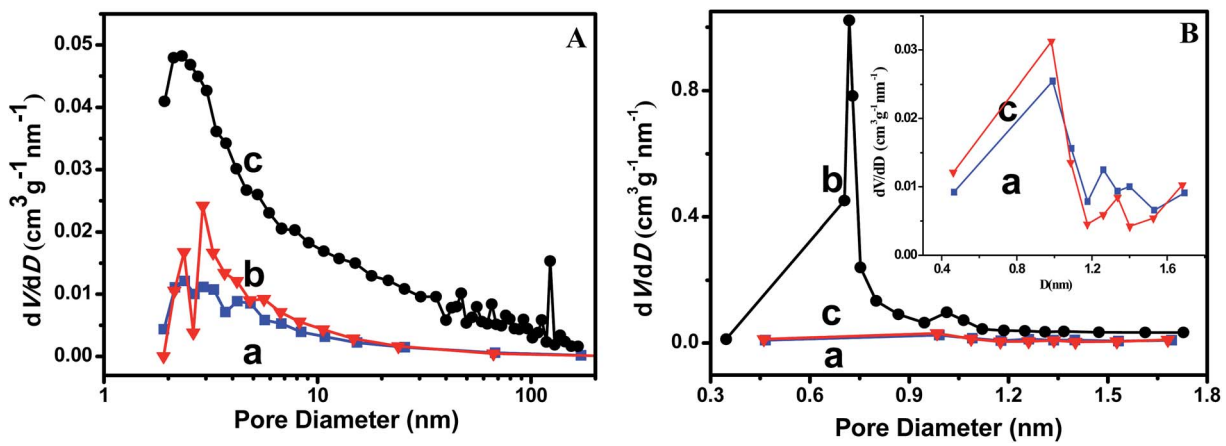

Fig. 5 BJH pore size distribution (A) and HK micropore size distribution (B) of samples: (a) NPC-723, (b) NPC-873 and (c) NPC-1173.

template from zeolite ZSM-39 and the mesopores may be derived from partially destroyed microstructures. The BET surface area of the NPC-873 sample reached up to 269.4 $m^2 g^{-1}$, implying that a suitable temperature was critical to obtain the carbon material with an ideal surface area. The total pore volume was calculated as 1.112 $cm^3 g^{-1}$ for NPC-873. Its pore diameter was mainly centered at about 3.0 nm, as obtained from the pore size distribution (Fig. 5Ab), which was similar to that of NPC-723. However, the number of pores was considerably larger than that of NPC-723, as seen from the changes in pore volume (Table 1), indicating that high temperature carbonization was beneficial to the exposure of mesopores. Along with the micropore centered at 1.0 nm (Fig. 5Bb), new micropore with the diameter centered at 0.72 nm was also exhibited, implying that more micropores were exposed as a result of the carbonization at 873 K. However, prominent changes were observed for NPC-1173 (Fig. 4c), implying pore evolutions of NPCs. Moreover, BET surface area decreased to 51.0 $m^2 g^{-1}$.

As depicted in Fig. S1,† it can be seen that the carbonization temperature had a great influence on the morphology of the obtained NPCs. The overall morphology of NPC-723 was a sintered carbon with an irregular morphology (Fig. S1A and D†). The particle size was about 50 × 30 μm. NPC-873 exhibited a fluffy, cotton-like morphology (Fig. S1B and E†), implying its highly developed pore structure. The particle size of NPC-873 was about 25 × 20 μm, which was slightly smaller than that of NPC-723. In addition, NPC-1173 was a uniform carbon sphere of about 1.5 μm in diameter (Fig. S1C and F†), which was evidently different from the NPC-723 and NPC-873. The changed morphology and particle size imply that the zeolite ZSM-39 melted into small spheres at a carbonization temperature of 1173 K. After the removal of SiO_2, carbon spheres were completely exposed, which may have resulted in the low specific surface area of NPC-1173, consistent with the results from N_2 isotherms. Therefore, a moderate carbonization temperature was necessary for obtaining materials with the desired surface area.

The sample NPC-873 was selected to evaluate thermal stability by recording its TG curves in air. Only a slight weight loss of 0.52% was observed below 100 °C (Fig. S2†), coinciding with the removal of physically adsorbed water. A weight loss about 0.32% was further observed in the range from 100 to 150 °C, which can be ascribed to trace dehydration. The decomposition of an N-containing group basically occurred in the range of 150–365 °C, which yielded an evident weight loss of 5.62%. Main weight loss of more than 90% ascribed to the ignition of carbon species was recorded above 365 °C. According to the DTG curve, the onset of the ignition temperature was around 465 °C. The samples NPC-723 and NPC-1173 showed the onset temperature at 385 °C and 615 °C (not shown here), respectively. Combining this data with the above XRD and Raman results, it was reasonable to conclude that the onset of the ignition temperature depended on the degree of graphitization based on the carbonization treatment. In addition, all of the results confirmed the presence of N atoms that were determined from FT-IR and elemental analysis.

In several cases, gas mixtures are mainly composed of acidic and inert gases. The N-containing functional groups are Lewis-base sites and are active for binding acidic molecules such as SO_2, H_2S, CO and CO_2. Herein, the adsorption selectivity of CO_2 and N_2 was selected as a reference and evaluated by comparing their uptake capacity at 293 K and 0.93 bar. The NPC-723 sample showed a CO_2 uptake capacity of 1.09 mmol g^{-1} (Fig. 6A). On the other hand, its N_2 uptake capacity was only 0.09 mmol g^{-1}. Accordingly, the adsorption selectivity of CO_2 over N_2 was estimated to be about 12.1. Since the kinetic diameter of CO_2 (0.33 nm) is smaller than that of N_2 (0.364 nm), the unique micropores in NPCs were accessible to CO_2 but not N_2 and mainly contributed to the excellent selectivity. This property makes NPC-723 a good candidate for separating low concentrations of CO_2 in the purification of gas mixtures.

The CO_2 uptake capacities of NPC samples at different temperatures were systematically investigated. At pressures up to 0.93 bar, the CO_2 adsorption isotherms of NPC samples were collected at 253, 273, and 293 K, respectively. As shown in Fig. 6B, all NPC samples showed the highest CO_2 uptake at a low temperature of 253 K because the kinetic energy of CO_2 molecules was small at this temperature. The NPC-723 sample showed the largest CO_2 uptake of 1.93, 1.42, and 1.09 mmol g^{-1} at 253, 273 and 293 K at 0.93 bar, respectively (Fig. 6Ba, Ca and Da). It exhibited an obvious uptake at a pressure of $P \leq 0.05$ bar, implying that the micropores were capable of good adsorption. However, the uptake capacity of NPC-723 gradually decreased with elevating temperatures from 253 K to 293 K, implying the physical sorption of CO_2.

Compared with samples NPC-873 and NPC-1173, the NPC-723 material exhibited the highest CO_2 uptake at the three different temperatures in spite of its low BET surface area (S_{BET} = 53.3 $m^2 g^{-1}$). This result may be due to its high N content of 18.14%. Although NPC-873, with an N content of 13.04%, had the highest BET surface area of 269.4 $m^2 g^{-1}$, which was 5 times higher than that for NPC-723, it only showed a moderate CO_2 uptake of 1.38, 0.91, and 0.85 mmol g^{-1} under the same conditions (Fig. 6Bb, Cb and Db). The results implied that the N element in samples played a more important role than the surface area. The NPC-1173 sample had a BET surface area similar to NPC-723 (Table 1), but it had the poorest CO_2 uptake capacity of 0.85, 0.84, and 0.46 mmol g^{-1} under the given conditions (Fig. 6Bc, Cc and Dc), which is understood because of its minimum N content. Overall, higher N contents of NPC materials result in higher CO_2 adsorption capacities. For example, the CO_2 adsorption capacity ratio at 253 K of sample NPC-723 to NPC-873 was about 1.398, which is close to their N content ratio of 1.391. These results indicate that the N-containing functional groups play a dominate role on the adsorption capacity of materials.

To explain the evolution of adsorption capacity, the nature of functional groups on the surface of the NPC materials was further studied using X-ray photoelectron spectroscopy (XPS). From the XPS survey spectra, all of the samples showed N1s and C1s peaks (Fig. 7a–d). It can be seen that the N contents of NPCs decreased with an increase in the carbonization temperature (Fig. 7b–d), which is coincident with the above elemental

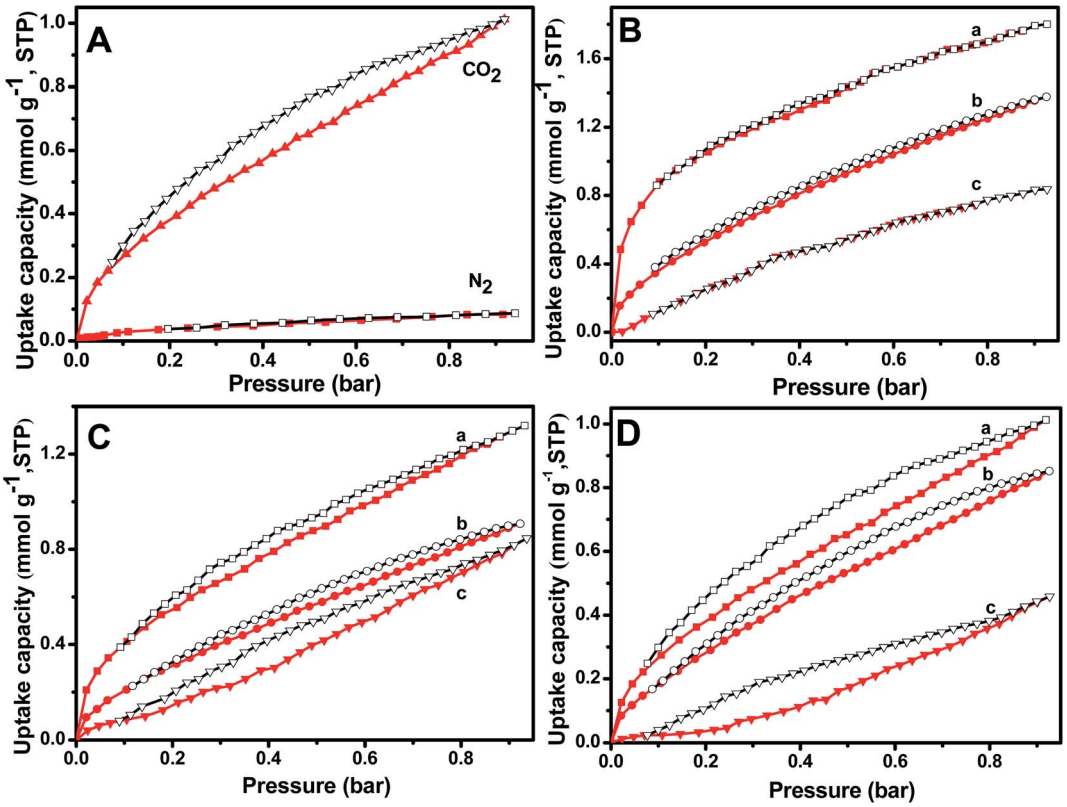

Fig. 6 N_2/CO_2 isotherms (adsorption branch in red and desorption in black) of sample NPC-723 at 293 K (A) and CO_2 isotherms of samples NPC-723 (a), NPC-873 (b) and NPC-1173 (c) at different temperatures: 253 K (B), 273 K (C) and 293 K (D).

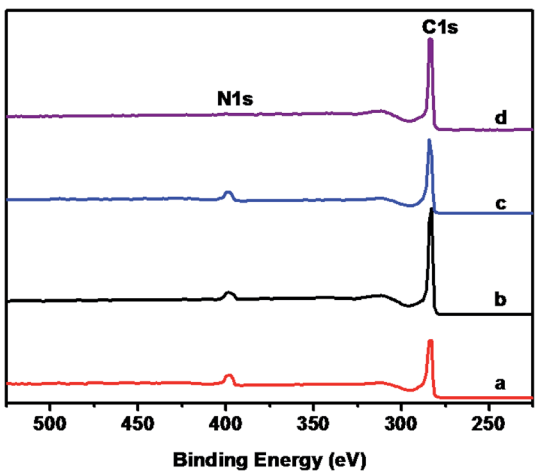

Fig. 7 XPS survey spectra of samples: (a) as-made zeolite ZSM-39, (b) NPC-723, (c) NPC-873, and (d) NPC-1173.

analysis results listed in Table 1. Particularly, no significant N1s peak was observed for NPC-1173 due to its high carbonization temperature (Fig. 7d). In the N1s spectra of all samples (Fig. S3†), the as-prepared zeolite ZSM-39 showed a strong peak at 401.1 eV, corresponding to the quaternary N of the organic template TMACl (Fig. S3a†).[31] After carbonization at 723 K, two new peaks at 397.9 and 400.4 eV were observed for the NPC-723 sample along with the decaying peak at 401.1 eV (Fig. S3b†). The former can be indexed to a pyridinic-type and pyrrolic/pyridonic N, respectively.[31] These results indicate the decomposition of the trapped template, TMACl, and the formation of new nitrogen species. The existence of quaternary, pyridinic, and pyrrolic/pyridonic N may alter the electron distribution and surface polarity of the carbon surface. The NPC-873 clearly exhibited two intense peaks at 397.9 and 400.4 eV (Fig. S3c†), corresponding to pyridinic-type and pyrrolic/pyridonic N, respectively. Essentially, the shoulder peak at 400.9 eV, corresponding to the quaternary N, was observed in NPC-873, which originated from the organic template, TMACl. The pyrolysis at 1173 K resulted in the disappearance of peaks indexed to pyridinic-type and pyrrolic/pyridonic N.[31] NPC-1173 only displayed a weak peak of quaternary N (Fig. S3d†), which is the most stable nitrogen group in NPC materials. The results mean that the occurrence of the de-nitrogenation agreed with the decreasing CO_2 adsorption capacity.

According to the results mentioned above, a material with high surface area does not always show a proportionally high CO_2 uptake capacity just as initially expected. Textual properties including internal surface area, pore structure, and functional groups may have different contributions on various adsorbates. Herein, the CO_2 adsorption capacity per unit surface area was proposed to be evaluated by calculating the CO_2 uptake capacity of the unit surface area defined by the BET surface area. As shown in Fig. 8, the CO_2 uptake capacity per unit surface area was calculated as 26.6 μmol m^{-2} for NPC-723 at 0.93 bar and

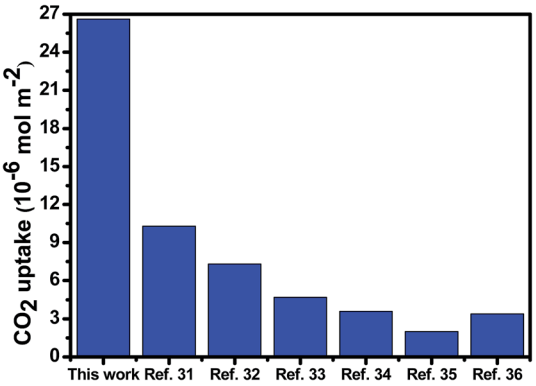

Fig. 8 The CO_2 adsorption capacities of a specific surface area for the NPC-723 sample in this study and several recently reported porous carbon adsorbents. The CO_2 adsorption capacities were collected at 0.93 bar and 273 K.

273 K, which is the best value among various recently reported CO_2 adsorbents. Most of the NPCs prepared using different procedures displayed poor to moderate CO_2 uptake capacity per unit surface area of 2–10.3 μmol m^{-2}, which were evidently lower than that of NPC-723 in this study. For example, NPCs prepared from a high surface area, microporous imine-linked polymer by direct pyrolysis showed a CO_2 uptake capacity per unit surface area of 10.3 μmol m^{-2} (Fig. 8).[31] The N-containing carbon framework carbonized from self-assembly of poly(benzoxazine-*co*-resol) showed a CO_2 uptake capacity per unit surface area of 7.3 μmol m^{-2} (Fig. 8).[32] Porous carbon prepared by chemical activation of hydrothermally carbonized polysaccharides only showed a CO_2 uptake capacity per unit surface area of 4.7 μmol m^{-2} (Fig. 8).[33] In addition, N-doped polypyrrole-based carbons showed a CO_2 uptake capacity per unit surface area of 3.6 μmol m^{-2}.[34] NPC templated from zeolite EMC-2 showed a poor CO_2 uptake capacity per unit surface area of 2.0 μmol m^{-2}.[35] Even highly porous N-doped polyimine-based carbons showed only a value of 3.4 μmol m^{-2}.[36] All the results implied that the surface area of the NPC-723 sample was fairly effective in capturing CO_2 even though the CO_2 uptake capacity was still lower than the carbon-based materials reported by other researchers.

Based on the above results, we concluded that the zeolite-cage-lock strategy for the formation of NPC mainly underwent the following steps: preparation of the zeolite, carbonization, and silica removal (Fig. 9). The zeolite ZSM-39 was hydrothermally synthesized with an initial mixture containing colloidal SiO_2, TMACl, H_2O, NH_4F and NaOH. TMACl acted as a structure-directing agent for the formation of zeolite and was simultaneously encapsulated into the zeolite cages.[37] Subsequently, the as-made zeolite ZSM-39 was directly carbonized in an argon flow at high temperature. Both C and N species were successfully locked in the zeolitic cage because of the limitation of its small pore windows. Moreover, both elemental analysis and FT-IR results confirmed the existence of N-containing species. In addition, some graphitization process occurred during the carbonization, implying the production of new bonds between C species. After the removal of silica, micropores of NPC, with a critical size between the dynamic diameter of CO_2 and N_2, were fabricated using the zeolite cage-lock strategy. Basic site derived from the N species was located in the ultramicropores of NPC. NPC displayed good selective adsorption and a high CO_2 adsorption capacity. Compared to the conventional chemical vapor deposition carried out in a zeolite, our approach to prepare NPC in one-step from an organic template trapped in the cage of a selected zeolite was more economical and simple for mass production. The strategy can be extended to synthesize sulfur-containing porous carbon and other materials.

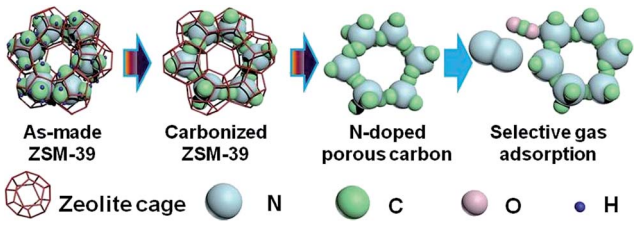

Fig. 9 Proposed formation mechanism and selective gas adsorption of N-doped porous carbon using a zeolite cage-lock strategy.

4. Conclusions

In this study, NPC materials were prepared by *in situ* carbonization of the organic template TMACl trapped in the cages of zeolite ZSM-39. The materials showed variable N contents (~1.11% to 18.14%) with different carbonization temperatures. The quaternary N from template TMACl was gradually transformed into pyridinic and pyrrolic/pyridonic N during the carbonization process. The NPC-723 sample with a high N content showed the highest CO_2 uptake values of 1.09, 1.42 and 1.93 mmol g^{-1} at 293, 273 and 253 K at 0.93 bar among the tested materials, respectively. The calculated CO_2 adsorption capacity per unit surface area for NPC-723 was 26.6 μmol m^{-2} at 0.93 bar and 273 K, which is the highest value among the reported carbon adsorbents. The adsorption selectivity of CO_2 over N_2 was more than 12.1 (molar ratio). Its excellent selectivity makes the NPC material a good candidate for the separation of low concentration CO_2 in the purification of gases.

Acknowledgements

The authors acknowledge the financial support provided by the China Scholarship Council (No. 201506935028), the National Natural Science Foundation of China (No. 21476156), the Natural Science Foundation of Shanxi Province (No. 2014011012-5), the Key Scientific and Technological Projects of Shanxi Province (No. MD2014-09), and the Talents Foundation of Taiyuan University of Technology (No. TYUT-RC201113A).

References

1 D. M. D'Alessandro, B. Smit and J. R. Long, Carbon dioxide capture: Prospects for new materials, *Angew. Chem., Int. Ed.*, 2010, **49**, 6058–6082.

2 A. Yamasaki, An overview of CO_2 mitigation options for global warming-emphasizing CO_2 sequestration options, *J. Chem. Eng. Jpn.*, 2003, **36**, 361–375.
3 S. Choi, J. H. Drese and C. W. Jones, Adsorbent materials for carbon dioxide capture from large anthropogenic point sources, *ChemSusChem*, 2009, **2**, 796–854.
4 J. Pawlesa, A. Zukal and J. Čejka, Synthesis and adsorption investigations of zeolites MCM-22 and MCM-49 modified by alkali metal cations, *Adsorption*, 2007, **13**, 257–265.
5 R. V. Siriwardane, M. S. Shen and E. P. Fisher, Adsorption of CO_2 on zeolites at moderate temperatures, *Energy Fuels*, 2005, **19**, 1153–1159.
6 Z. Yong, V. Mata and A. E. Rodrigues, Adsorption of carbon dioxide at high temperature: A review, *Sep. Purif. Technol.*, 2002, **26**, 195–205.
7 S. C. Lee, H. J. Chae, S. J. Lee, B. Y. Choi, C. K. Yi, J. B. Lee, *et al.*, Development of regenerable MgO-based sorbent promoted with K_2CO_3 for CO_2 capture at low temperatures, *Environ. Sci. Technol.*, 2008, **42**, 2736–2741.
8 J. Liu, P. K. Thallapally, B. P. McGrail, D. R. Brown and J. Liu, Progress in adsorption-based CO_2 capture by metal–organic frameworks, *Chem. Soc. Rev.*, 2012, **41**, 2308–2322.
9 K. Sumida, D. L. Rogow, J. A. Mason, T. M. McDonald, E. D. Bloch, Z. R. Herm, *et al.*, Carbon dioxide capture in metal–organic frameworks, *Chem. Rev.*, 2012, **112**, 724–781.
10 R. Banerjee, A. Phan, B. Wang, C. Knobler, H. Furukawa, M. O'Keeffe, *et al.*, High-throughput synthesis of zeolitic imidazolate frameworks and application to CO_2 capture, *Science*, 2008, **319**, 939–943.
11 C. F. Xue, B. Tu and D. Y. Zhao, Facile fabrication of hierarchically porous carbonaceous monoliths with ordered mesostructure *via* an organic organic self-assembly, *Nano Res.*, 2009, **2**, 242–253.
12 C. F. Xue, B. Tu and D. Y. Zhao, Evaporation-induced coating and self-assembly of ordered mesoporous carbon-silica composite monoliths with macroporous architecture on polyurethane foams, *Adv. Funct. Mater.*, 2008, **18**, 3914–3921.
13 R. Ryoo, S. H. Joo, M. Kruk and M. Jaroniec, Ordered mesoporous carbons, *Adv. Mater.*, 2001, **13**, 677–681.
14 C. O. Ania, V. Khomenko, E. Raymundo-Pinero, J. B. Parra and F. Beguin, The large electrochemical capacitance of microporous doped carbon obtained using a zeolite template, *Adv. Funct. Mater.*, 2007, **17**(11), 1828–1836.
15 D. Lozano-Castello, D. Cazorla-Amoros and A. Linares-Solano, Powdered activated carbons and activated carbon fibers for methane storage: A comparative study, *Energy Fuels*, 2002, **16**, 1321–1328.
16 J. P. Boudou, P. Parent, F. Suarez-Garcia, S. Villar-Rodil, A. Martinez-Alonso and J. M. D. Tascon, Nitrogen in aramid-based activated carbon fibers by TPD, XPS and XANES, *Carbon*, 2006, **44**, 2452–2462.
17 A. Castro-Muniz, F. Suarez-Garcia, A. Martinez-Alonso and J. M. D. Tascon, Activated carbon fibers with a high content of surface functional groups by phosphoric acid activation of PPTA, *J. Colloid Interface Sci.*, 2011, **361**, 301–315.
18 Z. Yang, Y. Xia, X. Sun and R. Mokaya, Preparation and hydrogen storage properties of zeolite-templated carbon materials nanocast *via* chemical vapor deposition: Effect of the zeolite template and nitrogen doping, *J. Phys. Chem. B*, 2006, **110**, 18424–18431.
19 Y. Xia and R. Mokaya, Generalized and facile synthesis approach to N-doped highly graphitic mesoporous carbon materials, *Chem. Mater.*, 2005, **17**, 1553–1560.
20 B. Zhu, K. Li, J. Liu, H. Liu, C. Sun, C. E. Snape, *et al.*, Nitrogen-enriched and hierarchically porous carbon macro-spheres – ideal for large-scale CO_2 capture, *J. Mater. Chem. A*, 2014, **2**, 5481–5489.
21 Z. Wu, P. A. Webley and D. Zhao, Post-enrichment of nitrogen in soft-templated ordered mesoporous carbon materials for highly efficient phenol removal and CO_2 capture, *J. Mater. Chem.*, 2012, **22**, 11379–11389.
22 H. Wang, Q. Gao and J. Hu, Preparation of porous doped carbons and the high performance in electrochemical capacitors, *Microporous Mesoporous Mater.*, 2010, **131**, 89–96.
23 P. X. Hou, H. Orikasa, T. Yamazaki, K. Matsuoka, A. Tomita, N. Setoyama, *et al.*, Synthesis of nitrogen-containing microporous carbon with a highly ordered structure and effect of nitrogen doping on H_2O adsorption, *Chem. Mater.*, 2005, **17**, 5187–5193.
24 Y. Xia, G. S. Walker, D. M. Grant and R. Mokaya, Hydrogen storage in high surface area carbons: experimental demonstration of the effects of nitrogen doping, *J. Am. Chem. Soc.*, 2009, **131**, 16493–16499.
25 A. Huang and J. Caro, Fabrication of MTN-type zeolite by self-assembling of supramolecular compound, *J. Cryst. Growth*, 2009, **311**, 4570–4574.
26 C. F. Xue and T. T. Xu, Fluorine-free synthesis of large ZSM-39 crystals incorporated with alkaline earth metals in an environment-friendly system, *Mater. Lett.*, 2013, **112**, 200–202.
27 Y. Xia and R. Mokaya, Synthesis of ordered mesoporous carbon and nitrogen-doped carbon materisla with graphitic pore walls *via* a simple chemical vapor deposition method, *Adv. Mater.*, 2004, **16**, 1553–1558.
28 X. L. Wu, T. Wen, H. L. Guo, S. B. Yang, X. K. Wang and A. W. Xu, Biomass derived sponge-like carbonaceous hydrogels and aerogels for supercapacitors, *ACS Nano*, 2013, **7**, 3589–3597.
29 S. Gunasekaran and B. Anita, Spectral investigation and normal coordinate analysis of piperazine, *Indian J. Pure Appl. Phys.*, 2008, **46**, 833–838.
30 K. J. Rothschild and H. Marrero, Infrared evidence that the Schiff base of bacteriorhodopsin is protonated: bR570 and K intermediates, *Proc. Natl. Acad. Sci. U. S. A.*, 1982, **79**, 4045–4049.
31 J. Wang, I. Senkovska, M. Oschatz, M. R. Lohe, L. Borchardt, A. Heerwig, *et al.*, Imine-linked polymer-derived nitrogen-doped microporous carbons with excellent CO_2 capture properties, *ACS Appl. Mater. Interfaces*, 2013, **5**, 3160–3167.
32 G. P. Hao, W. C. Li, D. Qian, G. H. Wang, W. P. Zhang, T. Zhang, *et al.*, Structurally designed synthesis of mechanically stable poly(benzoxazine-co-resol)-based porous carbon monoliths and their application as high-performance CO_2 capture sorbents, *J. Am. Chem. Soc.*, 2011, **133**, 11378–11388.

33 M. Sevilla and A. B. Fuertes, Sustainable porous carbons with a superior performance for CO_2 capture, *Energy Environ. Sci.*, 2011, **4**, 1765–1771.
34 M. Sevilla, P. Valle-Vigón and A. B. Fuertes, N-doped polypyrrole-based porous carbons for CO_2 capture, *Adv. Funct. Mater.*, 2011, **21**, 2781–2787.
35 Y. Xia, R. Mokaya, D. M. Grant and G. S. Walker, A simplified synthesis of N-doped zeolite-templated carbons, the control of the level of zeolite-like ordering and its effect on hydrogen storage properties, *Carbon*, 2011, **49**, 844–853.
36 J. Wang, I. Senkovska, M. Oschatz, M. R. Lohe, L. Borchardt, A. Heerwig, *et al.*, Highly porous nitrogen-doped polyimine-based carbons with adjustable microstructures for CO_2 capture, *J. Mater. Chem. A*, 2013, **1**, 10951–10961.
37 J. L. Schlenker, F. G. Dwyer, E. E. Jenkins, W. J. Rohrbaugh and G. T. Kokotailo, Crystal structure of a synthetic high silica zeolite–ZSM-39, *Nature*, 1981, **294**, 340–342.